

**Effects of Sea Water pH on Marine Mussel Plaque Maturation**

|                               |  |
|-------------------------------|--|
| Journal:                      | <i>Soft Matter</i>   |
| Manuscript ID                 | SM-ART-07-2020-001237.R1   |
| Article Type:                 | Paper  |
| Date Submitted by the Author: | 26-Aug-2020  |
| Complete List of Authors:     | Bernstein, Justin; University of California Santa Barbara, College of Creative Studies<br>Filippidi, Emmanouela; Max-Planck-Institute of Molecular Cell Biology and Genetics,<br>Waite, Herbert; University of California Santa Barbara, Department of Molecular, Cell & Developmental Biology<br>Valentine, Megan; University of California Santa Barbara, Mechanical Engineering |
|                               |  |

## ARTICLE

## Effects of Sea Water pH on Marine Mussel Plaque Maturation

Justin H. Bernstein<sup>a</sup>, Emmanouela Filippidi<sup>b,c,§</sup>, J. Herbert Waite<sup>c,d</sup>, Megan T. Valentine<sup>b,c,†</sup>Received 00th January 20xx,  
Accepted 00th January 20xx

DOI: 10.1039/x0xx00000x

Marine mussel plaques are an exceptional model for wet adhesives. Despite advances in understanding their protein composition and strategies for molecular bonding, the process by which these soluble proteins are rapidly processed into load-bearing structures remains poorly understood. Here, we examine the effects of seawater pH on the time evolution of the internal microstructures in plaques harvested from *Mytilus californianus*. Experimentally, plaques deposited by mussels on glass and acrylic surfaces were collected immediately after foot retraction without plaque separation from the surface, placed into pH-adjusted artificial seawater for varying times, and characterized using scanning electron microscopy and tensile testing. We found a pH dependent transition from a liquid-like state to a porous solid within 30 minutes for pH  $\geq$  6.7; these plaques are load-bearing. By contrast, samples maintained at pH 3.0 showed no porosity and no measurable strength. Interestingly, we found cuticle development within 15 min regardless of pH, suggesting that cuticle formation occurs prior to pore assembly. Our results suggest that sea water infusion after deposition by and disengagement of the foot is critical to the rapid formation of internal structures, which in turn plays an important role in the plaques' mechanical performance.

## 1. Introduction

Marine mussels have the remarkable ability to adhere to rocks and each other within the wave-swept intertidal zone, using a series of collagen-enriched threads that terminate in adhesive plaques comprised of a spongy, porous interior and hard external cuticle which covers both the plaque and thread<sup>1-4</sup>. The radial array of plaque-thread structures formed by each mussel, known as the byssus, is continuously renewed by addition and replacement of damaged plaque-thread structures, providing the mussel with strong, tenacious adhesion<sup>5, 6</sup>. Mussel plaques, which adhere directly to their substrates in hostile ocean environments, are of particular interest because of their ability to form quickly (within minutes), cure underwater, and withstand relatively high tensile stresses<sup>7-10</sup>.

Mussel plaque formation is an extraordinary example of biomaterial processing. Mussels generate precursor materials in advance, package them in granules, and store them within gland reservoirs within the mussel body<sup>11-14</sup>. Upon demand, the precursors migrate to the ventral groove of the mussel foot, a strong and conformable external organ that is used in

locomotion, but also serves a critical role in byssus manufacturing<sup>15, 16</sup>. The foot provides a strong seal to the substrate, and the granules are released in a time-gated fashion through the ventral groove to generate the byssal thread and plaque in a process that resembles industrial injection moulding. This fabrication process is rapid, taking 0.5–8 minutes from initiation to foot retraction per thread<sup>15, 17</sup>.

Although much is known about the composition and biochemistry of the proteins present in mussel plaques<sup>3, 15</sup>, a detailed understanding of the biomaterial processing, and how this processing relates to the mechanical performance of the byssal thread-plaque structures remains elusive. The prevailing model is that upon initiation, the mussel foot anchors to the surface forming a seal under the distal depression; plaque proteins are then deposited onto the substrate. Mussels actively control the pH, ionic strength, and redox conditions under the foot during deposition<sup>15, 17-19</sup>. Within this tightly controlled chemical environment, a series of specialized mussel foot proteins (mfp) are secreted at the phenol gland of the foot, with nearly all having calculated isoelectric points (pI) between 7.5 and 10.5<sup>3, 15, 20, 21</sup>. Several, including mfp-4, mfp-9, mfp-11 and mfp-12, contain large amounts, up to 25 mol-%, of histidine, which has a  $pK_a \sim 6$ ; these may impart particular sensitivity to the seawater pH.

Upon initiation of plaque formation, the distal depression is acidified to pH  $\sim 2-4$  and mfp-3, mfp-5, mfp-6, mfp-10, mfp-11 and mfp-12, mfp-15 are secreted to form the plaque body<sup>15, 17</sup>. It is believed that these condense via liquid-liquid phase separation, to form a metastable complex coacervate<sup>21, 22</sup>. The low interfacial energy, high internal diffusion coefficient, and shear-thinning viscosity of coacervates are highly advantageous in wetting the substrate<sup>23, 24</sup>. Although it has not been possible to directly observe coacervation during natural plaque formation, a number of mfps have been shown to coacervate *in*

<sup>a</sup> College of Creative Studies, University of California - Santa Barbara, Santa Barbara, CA, 93106, USA

<sup>b</sup> Materials Research Laboratory, University of California - Santa Barbara, Santa Barbara, CA, 93106, USA

<sup>c</sup> Department of Mechanical Engineering, University of California - Santa Barbara, Santa Barbara, CA, 93106, USA

<sup>d</sup> Molecular, Cellular and Developmental Biology, University of California - Santa Barbara, Santa Barbara, CA, 93106, USA

§ Current Address: Max Planck Institute for Physics of Complex Systems, Dresden, Germany

† Corresponding Author: valentine@engineering.ucsb.edu

Electronic Supplementary Information (ESI) available: [details of any supplementary information available should be included here]. See DOI: 10.1039/x0xx00000x

*vitro*<sup>21, 23, 25-27</sup>. This process has been shown to be pH-dependent: increased pH deprotonates acidic groups such as phosphate and carboxylic groups driving the formation of zwitterions which subsequently aggregate forming complex coacervates<sup>21</sup>.

Before or soon after foot retraction, this complex liquid phase must solidify to form the load-bearing microporous plaque we observe in final thread-plaque structures<sup>2, 3, 10</sup>. It has been proposed that the microscale porosity could arise from a phase inversion process, which may be triggered by the influx of sea water and accompanying pH inversion from low pH  $\sim 3$  at deposition to the relatively high pH ocean seawater pH  $\sim 8.2$  when the foot is withdrawn. The initial material comprises dispersed coacervate droplets in a continuous water phase<sup>28</sup>. A phase inversion, which has industrial use in forming microporous polymeric membranes for filtration<sup>29-31</sup>, would result in a continuous, protein-rich coacervate phase, with dispersed aqueous droplets. Presumably there is also an important role for time-gated crosslinking, which would provide mechanical elasticity and strength. Among the most prominent amino acids within the mfps are histidine, lysine, glycine, and 3,4-dihydroxyphenylalanine (Dopa), a modified form of tyrosine with two hydroxy groups located ortho to each other on the substituted benzene ring<sup>15, 32</sup>. Previous studies have demonstrated that pH mitigates quinone-based cross-linking and catechol-mediated metal-ion coordinate bonding<sup>3, 17</sup>. At low pH the hydroxy groups are protonated allowing for mono coordinated metal ion coordination and hydrogen bonding<sup>15, 33-35</sup>. In this regime, electrostatic and hydrophobic interactions dominate. As pH increases (to  $\sim$  pH 8), the hydroxy substituents are oxidised forming Dopa-quinone, which allows for the formation of coordinated bidentate bonding. Similarly, pH dependent oxidation likely causes covalent cross-links with substituents such as cysteine<sup>36</sup>. Both bond structures likely contribute to the development of cohesive strength within the plaque body, and adhesive strength between the plaque and the substrate<sup>17, 18</sup>.

Such phase inversion and solidification has been demonstrated *in vitro* with a mussel-inspired coacervated material<sup>37</sup>, but direct observation of such events within the natural system has proven extremely challenging. This is largely due to the severe experimental limitations on studying plaque formation *in situ*, including the random initiation process, extremely rapid processing times, plaque turbidity, the sensitivity of the mussel to changes in ambient light during plaque deposition and the fact that deposition, self-assembly and solidification occur under the mussel foot, precluding simple observations of the process. Though the exact sequence of events is not known with certainty, it is believed that rapid change in pH is key to the generation of physically robust mussel plaques<sup>17</sup>, which are called into mechanical service immediately upon formation.

Here, we focus on the critical role of environmental pH in mussel plaque maturation. We hypothesize that the rapid influx of seawater (commonly at pH  $\sim 8$ ) to the newly formed plaques brings the mfps within range of their isoelectric point<sup>38</sup> and drives the formation of the porous plaque microstructure. To

test this, we surreptitiously observed *Mytilus californianus* mussels submerged in filtered sea water at pH  $\sim 8.0$  in a laboratory tank environment as they naturally produce new byssal thread-plaques. Nascent thread-plaques were immediately collected, within 5 min of deposition, and placed in pH-adjusted artificial sea water (ASW) solutions for varying amounts of time. Imaging and mechanical testing were used to examine the maturation of the microstructures that form the porous plaque interior and cuticle, as well as the impact of structural maturation on plaque mechanics and adhesion strength. By studying the pH-dependent kinetics of structural formation, we can gain insight into the role of pH on the evolution of micro-structures, and the sequence of bioprocessing.

## 2. Experimental Methods

**2.1 Collecting Plaques and Preparing Samples.** Mussels (*Mytilus californianus*; Conrad, 1837) were collected from the intertidal zone off the coast of Goleta, CA and placed in tanks with continuously circulating filtered seawater at a temperature of  $\sim 12^\circ\text{C}$ . Immediately before experiments, mussels (typical adult length  $\approx 10$  cm) were subjected to breaking waves at the beach for 30 min to stimulate plaque production and returned to the lab. Before placement in the mariculture tank, each mussel was secured *via* rubber bands to large acrylic (Plexiglas) plates. Each large plate was tiled with either small acrylic slides, for SEM imaging, or smaller glass slides, for tensile testing. Mussels deposited their thread-plaque structures directly onto the slides. Mussels were visually monitored before and during plaque deposition. Immediately after foot retraction, which signals the end of plaque manufacturing, the thread-plaque structures were removed from the mussel by cutting the threads near the distal end of the byssal thread with a razor blade. The collected plaques, still attached to the acrylic or glass slides, were then placed into artificial seawater (ASW) solutions (420 mM NaCl, 9.4 mM KCl, 25 mM  $\text{MgSO}_4 \cdot 7\text{H}_2\text{O}$ , 22 mM  $\text{MgCl}_2$ , 9 mM  $\text{CaCl}_2$  and 2.38 mM  $\text{NaHCO}_3$ ) with pH adjusted to 3.0, 6.7, or 7.8 for an appropriate duration of time in the range of 15 min to 24 hrs, based on the experiment. The pH of the ASW solutions was adjusted by adding HCl. Samples were kept at  $\sim 12^\circ\text{C}$  during ASW submersion, the same temperature as in the circulating tanks.

In all cases, we waited at least 15 minutes after collection before fixing the samples. Mussels can be uncooperative participants and are very sensitive to their local environmental conditions, so we attempt observe them with minimal disruption, and intervene to collect their plaques as soon as possible after the foot is fully retracted. Reliably collecting specimens within 5 minutes is challenging, and there is some error in timing the exact moment of foot retraction. This error necessarily becomes a larger fraction of the total time for shorter submersion periods, and we felt 15 minutes was the smallest time period we could reliably study.

A subset of thread-plaque structures was subjected to stepwise changes in pH to further investigate the pH- and time-dependent evolution of microstructure. Four different pH

treatments were tested by submersion in ASW as follows: (1) 30 min at pH 3.0 followed by 24 hrs at pH 7.8; (2) 24 hrs at pH 3.0 followed by 24 hrs at pH 7.8; (3) 30 min at pH 7.8 followed by 24 hrs at pH 3.0; and (4) 24 hours at pH 7.8 followed by 24 hrs at pH 3.

**2.2 Scanning Electron Microscopy.** After submersion for the desired time, the still-attached thread-plaque structures were rinsed with Milli-q water to remove residual ASW solution and placed in an aqueous 2.5% glutaraldehyde, 3.7% formaldehyde solution for 2 hours to allow for fixation of the protein-rich structure. The plaques were then rinsed with water to remove residual fixative and detached from the acrylic slides using a razor blade. Individual plaques were embedded in Neg-50 cryoprotectant at  $-22^{\circ}\text{C}$  and sectioned using a microtome (Leica CM 1850) into 20- $\mu\text{m}$  thick slices. We oriented the plaques with their long axis parallel to the blade prior to slicing to enable comparisons of similar cross-sections; typically, the central slices with the largest interior areal fraction were selected for imaging. The slices were placed in Milli-Q water, rinsed several times to remove the embedding medium, then dehydrated through a series of solvent exchange steps from water to ethanol to hexamethyldisilazane (HMDS). All exchanges were performed in 10-min intervals, first with water:ethanol solutions at the following ratios 10:1, 5:1, 3:1 1:1, 1:4, 1:10, 0:1, followed by exchange into ethanol:HMDS solutions at ratios of 9:3, 1:1, 1:4. We have previously demonstrated that this preparation protocol does not disrupt the natural plaque ultrastructure by comparing the results obtained via SEM of fixed samples with those obtained via small-angle and ultra-small-angle neutron scattering of samples.<sup>2</sup> The samples were then mounted on scanning electron microscopy (SEM) stubs, sputter coated with gold/palladium 60/40, 99.99% (Hummer 6.2, Anatech, USA) for 100 s and imaged in secondary electron mode with a scanning electron microscope (ThermoFisher Apero C LoVac FEG SEM or FEI Nova Nano 650 FEG SEM) using accelerating voltages of 5 kV, or a spotting number of 4. All images were scaled to the desired magnification for post-processing.

**2.3 Pore Analysis.** For experimental conditions that produced plaques with measurable microscale pores (pH 6.7 and pH 7.8), SEM images were obtained as described above for the 15 min and 24 hr time points, and then analysed with Image J. Large images were cropped into smaller regions (with up to six subsections per image) for ease of visualization and measurement. Each subsection was manually thresholded to create binary images that distinguished the pixels representing the pore regions (voids) from those representing the continuous matrix. Pore areas were then measured using the built-in 'analyse particles' feature in ImageJ.

In some cases, thresholding led to the incorrect assignment of large regions enriched in collagen and/or regions containing high spatial-frequency noise to the 'pore' fraction. These incorrect assignments led to the inclusion of very large or very small areas, inconsistent with the areas of single pores. The erroneous assignments were removed from the pore area

distribution using a bandpass filter where the minimum and maximum pore area cut-off values were determined through manual analysis of representative images. The bandpass-filtered pore area data was averaged and the average values pooled; at each treatment condition 12-17 different SEM images were analysed giving 26-53 measured averages per treatment. To capture the natural range of pore structures present in the samples, images from a variety of regions within a single plaque and also from different plaques were used for each condition. See Figure S1-S3 for representative fields of view at each pH condition at the 24-hour time point.

Given the technical complexities of the current experiments, we did not complete a location-specific analysis of pore properties as a function of pH, but from our qualitative analysis of many images, we did not observe any trends that would suggest that pooling data from multiple plaques, or multiple regions within plaques, would be problematic. Moreover, prior analysis of the ultrastructure of mature plaques formed in natural seawater conditions showed no significant differences in the distributions of pore sizes or shapes measured at different locations within the plaque<sup>2</sup>. We have further confirmed that the microscale structural properties of plaques formed in natural, filtered seawater and artificial seawater at pH 7.8 are indistinguishable (Figure S4).

From the pooled processed image data, we calculated the average pore area per treatment as well as the average porosity, defined as the ratio of total pore area to total sample area. Pooled averages for each sample were compared using a one-way ANOVA to look for statistically significant differences in the measured average pore areas and porosities.

The data were represented using a boxplot. The lower limits of the box bounds represent the first quartile (25th percentile). Upper limits of the box bounds represent the third quartile (75th percentile). Thick horizontal lines represent the median. The black circular markers represent potential outliers. The \*\*\* markers represents  $p$  values of 0.001. The vertical lines represent the predicted minimum and maximum values of the data. These were determined by subtracting 1.5 times the inter quartile range (IQR) from the first quartile for the lower limit, and adding 1.5 times the IQR to the third quartile for the upper limit.

**2.4 Tensile Testing.** Mussel plaques were collected as described, using glass slides as a substrate. Immediately after collection, samples were placed in ASW solutions of pH 3.0, 6.7, or 7.8 at room temperature. Within  $\sim 1$  hr of collection, threads were secured to glass tubes (I.D. 0.69 mm; O.D. 1.2 mm) using a polyurethane-based waterproof glue (Gorilla Glue) to enable clamping during tensile testing. A short portion of thread was retained between the rod and plaque, typically  $\sim 6.5$  mm. The plaque structures were then submerged in their corresponding ASW solution, while the thread/rod joint was kept dry and the glue cured in air at room temperature for 22 - 24 hours. Unfortunately, this precludes mechanical testing of plaques at time points less than  $\sim 24$  hours after deposition.

After curing, uniaxial tensile testing was performed using a vertical TwinRail positioning table (Lintech, CA) with a Lebow

Load Cell (Model 3108-10, 10lb capacity, Eaton Corp., MI) fitted with a machined sample holder. Samples were removed from the ASW solution immediately prior to testing and the glass rod secured to the crosshead using a small self-centring drill chuck. This step was performed quickly (< 5 minutes) to retain as much moisture as possible within the plaque during testing. Each sample was tested in air with a pull angle of 45° and a pulling rate of 1.2mm/min, as measured from the crosshead motion. Force and crosshead displacement were measured as a function of time at a data sampling rate of 1 Hz, and all samples were loaded until failure. Videos were taken during testing, using a Canon Rebel SL2 (100 mm, f/2.8 Macro USM fixed lens, 1x magnification, 30 frames per second), to record the dynamics of detachment. Failure commonly occurred by one of three modes: cohesive failure within the plaque, adhesive failure at the plaque-glass interface, and failure at the thread-rod interface, likely due to stress concentrations associated with gluing. All failure modes were included in the analysis, consistent with previous studies<sup>10</sup>.

**2.5 Force-displacement analysis.** For each sample, the measured force was plotted as a function of crosshead displacement. The force sensor was zeroed per sample by determining the average measured force after failure (from ~30 time points); this value was then subtracted from all force data. At small displacements, the force-extension response for the plaque-thread structures is elastic<sup>9, 10</sup>. To determine the zero-force extension, a linear fit using least-squares regression to the force-extension data was performed over a range that maximized the  $r^2$  value, and the x-intercept subtracted from all extension data. Only positive values of extension were retained for analysis.

The measured force data,  $F$ , were normalized to account for differences in plaque sizes<sup>10</sup>. Images of the plaques were taken prior to testing using either a Canon Rebel SL2 camera or a Keyence VHX-5000 series microscope with a Keyence, VH-Z20R/Z20T lens. The diameter of the plaque was measured by taking images of each plaque, measuring the diameter both in width (minor axis,  $D_m$ ) and length (major axis,  $D_M$ ) with ImageJ, then calculating the plaque diameter from the geometric mean:  $D_p = \sqrt{D_m \times D_M}$ . For ease of comparison, all force data were normalized to that of a 'standard' plaque of diameter 2.5 mm:  $F^* = F \times 2.5\text{mm}/D_p$ .

All analyses were executed in MATLAB.

**2.6 Cuticle Thickness Measurements.** Samples were prepared for imaging using the methods described above. Cuticle thickness was then measured at each pH and time condition using the measurement tool in ImageJ. Manual measurements were made using 2-12 different images per condition taken from 1-2 different plaques resulting in a total number of measurements,  $n$ , which ranged from 78 to 3368 depending on the experiment defined by the pH and the ASW submersion time before fixation (Table S1). We define the cuticle region as the electron dense, pore-free interlayer just inside the outer plaque boundary (Figure S6). This is distinguished from the less dense inner region, which in some pH conditions contains

pores. An attempt was made to take evenly-spaced measurements across the specimen surface using lines normal to the outer cuticle boundary.

### 3 Results and Discussion

**3.1 pH Dependent Formation of the Inner Porous Foam.** To investigate the pH and time dependent formation of internal plaque structures, SEM images of plaques subjected to pH-adjusted artificial seawater (ASW) solutions for different submersion times were compared (Figure 1). Three pH conditions were tested. The lowest value of pH 3.0 is near the pH measured under the mussel foot during plaque deposition<sup>17</sup>. The pH 6.7 represents the lowest measured pH conditions in natural ocean environments<sup>38</sup>. Finally, pH 7.8 approached natural ocean conditions<sup>38</sup>.

In prior studies, we established the ultrastructural properties of mature plaques (at least several hours post-deposition) that were naturally-formed in filtered seawater<sup>2</sup>. Using SEM and neutron scattering, we demonstrated that the plaque interior resembles an open-cell reticulated foam with two characteristic length scales. One scale describes the pore diameter at 1–3  $\mu\text{m}$  and another describes the pore walls and struts at  $\sim 100$  nm. The pores were slightly elongated on average, with a ratio of major to minor axes of  $\sim 1.5$ . We found no significant differences in the distributions of pore sizes or aspect ratios measured at different locations within the plaque or as a function of mussel size.

In the current work, we present a comparative analysis of the microscale structures of plaques subjected to different pH conditions using multiple images at each condition using SEM. When freshly deposited plaques were introduced to ASW at pH  $\geq 6.7$ , porous structures are observed within 15 min (Figures 1, S5). The structures continue to rapidly evolve, leading to a more homogenous distribution of pores within 30 min of deposition; these pores remain visible for at least 24 hours. By contrast, freshly deposited plaques introduced to pH 3.0 ASW solutions never developed pores, even after 24 hrs of submersion (Figure 1), suggesting that at acidic pH values (near the deposition pH) the segregation of proteins into compartments was insufficient to induce phase separation. There is some evidence of disordered structure or texture in the images. These structures appear to have high variability and are consistent with structures observed in induced mussel plaques<sup>2</sup>. Taken together, our data suggest that the influx of higher pH seawater after plaque deposition and foot retraction is critical to proper bioprocessing through the pH-dependent phase separation of plaque proteins, which in turn drives the rapid formation of the porous microstructure.

Plaque structures under pore-forming conditions were analysed in greater detail by measuring the average pore area and average porosity, defined as the ratio of total pore area to total plaque area per image at 15 min and 24 hrs after deposition. Plaques at pH 3.0 were not analysed.

Both average pore area and average porosity increased with time and pH. The average pore area and porosity for plaques submerged at pH 6.7 increased from 0.83  $\mu\text{m}^2$  and 11 % at 15

min to  $1.04 \mu\text{m}^2$  and 17 % at 24 hrs (Figure 2A). Both values were determined to be significantly different using the Kruskal-Wallis Anova and Dunn non-parametric post-hoc tests ( $p < 0.001$ ). Similarly, for pH 7.8, the average pore area and porosity significantly increased from  $1.3 \mu\text{m}^2$  and 20 % at 15 min to  $3.3 \mu\text{m}^2$  and 28% at 24 hrs respectively (Figure 2B; Kruskal-Wallis Anova and Dunn post-hoc tests,  $p < 0.001$ ). These data suggest that pore area and porosity are strongly correlated, and that the pore structure coarsens over time, with larger pores developing at longer times for both pH conditions. Moreover, when we compared the structures formed under different pH conditions, we found that the average pore area and average porosity were significantly larger for pH 7.8 at all respective time points as compared to those formed at pH 6.7 (Kruskal-Wallis Anova and Dunn post-hoc tests,  $p < 0.001$ ). This suggests that even small differences in pH can affect structural formation.

The molecular origins of this pH- and time-dependent coarsening are not currently known. It has been demonstrated at least near the plaque:substrate interface the pores are likely filled with coacervate,<sup>28</sup> although it is possible that the liquid composition is not uniform throughout the plaque body. In coacervated solutions, it is not surprising that the polymer-rich droplets would grow in size or number with increasing pH, as these conditions are further from the critical point, and a higher volume fraction of phase-separated dense phase would be expected. The coarsening of the pore structure, which leads to an increase in average pore size, may follow this thermodynamic phase separation, and proceed through processes such as Ostwald ripening or droplet coalescence. It is also possible that the pH-dependent crosslinking reactions lead to a densification of the continuous matrix over time.

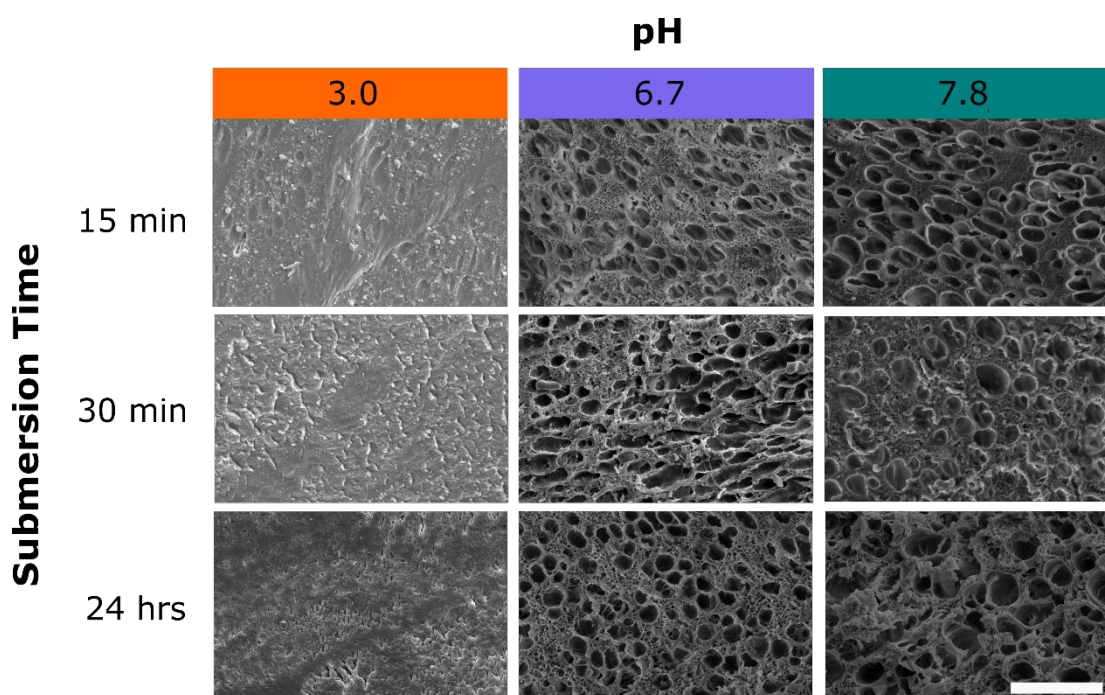


**Figure 1.** Scanning electron microscopy (SEM) images of the pH and time dependent structural evolution for plaques submerged in artificial seawater at pH 3.0, 6.7, and 7.8 for 15 min, 30 min, and 24 hours. Scale Bar is  $10 \mu\text{m}$ .

## ARTICLE

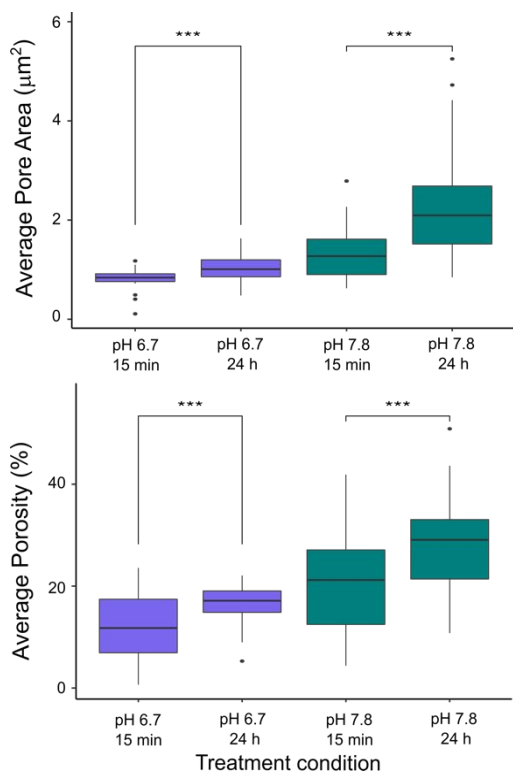


**Figure 2.** Average pore area (A) and average porosity (B) as a function of time for each pH condition.

**3.2 Reversibility of Structure Formation** To further investigate the effects of pH and time on the formation of the porous meshwork, plaques were subjected to stepwise changes in pH, and the resultant microstructures analysed by SEM. Four different pH treatments were tested and compared: (1) 30 min at pH 3.0 followed by 24 hrs at pH 7.8; (2) 24 hrs at pH 3.0 followed by 24 hrs at pH 7.8; (3) 30 min at pH 7.8 followed by 24 hrs at pH 3.0; and (4) 24 hours at pH 7.8 followed by 24 hrs at pH 3. By choosing to study the extremal values of pH 3.0 and 7.8 we explored the most dramatic effects of pH change on plaque properties.

First, we submerged the plaques into pH 3.0, a condition we know does not lead to pore formation, even after 24 hrs of submersion. However, if, after 30 minutes, the plaque is removed from the pH 3.0 solution, rinsed with DI water, and submerged into a normal seawater condition of pH 7.8, pores form (Figure 3A). Indeed, even after submersion of the plaque at pH 3.0 for 24 hrs, subsequent rinsing and submersion in pH 7.8 ASW leads to formation of pores (Figure 3B), although the pore structure that forms is more open in this case. Similarly, we can subject plaques

submerged in pH 7.8 solutions for 30 min or 24 hrs to submersion in pH 3.0 solutions and examine their internal microstructure (Figure 3C, 3D). When the plaque was submerged in pH 7.8 solution for only 30 minutes, and then returned to the deposition pH of 3.0, we found a significant disruption of the porous microstructure, suggesting that the crosslinking chemistries and self-assembly of the pores induced by influx of high pH seawater are not robust on this timescale and can be at least partially reversed upon return to the highly acidic conditions of deposition.

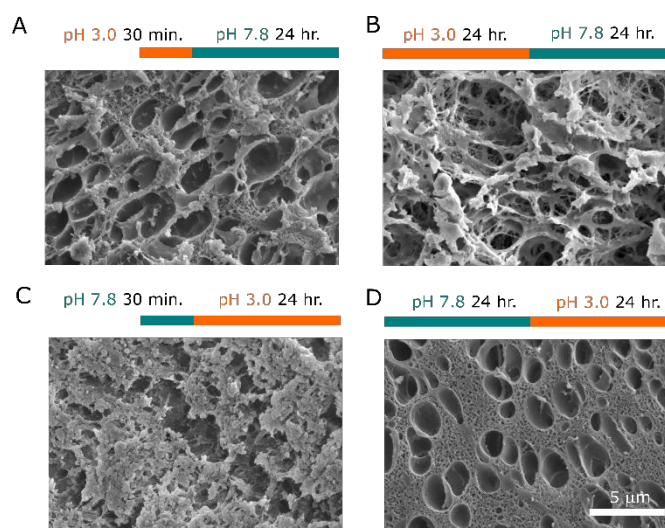


**Figure 3.** Representative SEM images of the interior spongy region of plaque subjected to stepwise changes in pH, with schedules indicated above each panel. Scale bar is 5 µm.

By contrast, if the plaques are maintained at pH 7.8 for 24 hours, and then returned to pH 3.0 for 24 hours, there is no obvious change in the size of the microscale pores, as compared to plaques that are never returned to pH 3.0 suggesting that the major cross-linking reactions leading to the pore boundary solidification have been completed by 24 hours. Importantly, all samples submerged at pH 7.8 for 24 hours, in any order, demonstrated the formation of a microporous meshwork. There is a hint of densification in the continuous matrix that surrounds the microscale pores for the plaque treated at pH 7.8 for 24 hours and then returned to acidic conditions for 24 hours (Fig 3D), although the level of natural variation in the mussel plaque samples is large (see Figures S1-S3) and our current measurements lack the resolution to discern subtle changes in plaque properties at submicron scales. In the future, neutron scattering experiments may provide additional insight.

**3.3 Cuticle formation** Thus far, we have focused on formation kinetics of the inner porous meshwork. However, the hard outer cuticle is also important to the adhesion performance and load-bearing properties of the byssal thread-plaque<sup>1</sup>. To understand how pH and time affect its structural development, we again use SEM to observe cuticle formation under varying experimental conditions. The thickness of plaque cuticles for pH 3.0, 6.7, and 7.8 were measured at 15 min, 30 min, and 24 hours. Average cuticle thickness measurements at each pH and time point ranged from  $\sim 3 \mu\text{m}$  to  $\sim 14 \mu\text{m}$  (Table S1; Figure S6). These are within range of previous studies on thread cuticle which measured a thickness of  $\sim 5 \mu\text{m}$ <sup>39</sup>. Cuticle formation appeared to be robust, forming with 15 min even at pH 3.0. This suggests that the cuticle may form before foot removal, perhaps to help provide mechanical strength and integrity while the inner porous meshwork has time to fully mature<sup>1</sup>.

Importantly, prior studies suggest that cuticle formation does not preclude solvent exchange: it has been demonstrated that the cuticle is highly hydrated,<sup>4</sup> and that the pH of plaque:substrate interface equilibrates with time.<sup>17</sup> Also, plaques in the natural environment appear to dry out when exposed during low tide, indicating that small molecule diffusion or transport can occur. Solvent exchange may arise from permeability within the cuticle wall itself to water or ions, or to the presence of an imperfect seal at the base of the plaque which enables water/ion transport, or both. No obvious trend in cuticle thickness with treatment conditions was observed, although we were unable to identify a distinct cuticle zone for the pH 3.0, 24 hr submersion time, which suggests that maintenance of this structurally-distinct zone may require pH-dependent crosslinking, although we cannot rule out the possibility that sustained exposures to acidic solutions could promote denaturation of the proteins forming the cuticle.

**3.4 pH Dependent Mechanical Strength.** Through analysis of electron micrographs of byssal thread-plaques subjected to various experimental treatments, we have shown that pH affects the formation of the internal porous microstructures, but not the outer cuticle. In order to assess the extent to which these changes affect function, mechanical tensile testing was performed. Due to the curing requirements of the adhesives used to affix the thread-plaque structures to glass rods that were in turn clamped to the tensile testing machine, only the 24 hr time mark was tested at each pH condition. In each case, plaques were affixed to the glass rods within 1 hour of deposition, and then allowed to set overnight to allow full glue curing.

Plaques at pH 3.0 were too feeble to measure: they were so weakly attached to the glass slides that it was impossible to adhere them to the glass rods for testing without causing plaque-glass detachment. We anticipate that at this deposition pH, amino acid substituents should be constantly protonated and likely initially form structures via electrostatic interactions (i.e. H-bonding) or predominantly mono-coordinated metal ion coordination, leading to the extremely weak nature of the plaques.<sup>33</sup> This is further supported by a recent study that found that at low pH and without fixatives, a substantial amount of

plaque material dissolves into constitutive proteins, suggesting a lack of substantial structural formation, consistent with our results.<sup>28</sup>

By contrast, plaques submerged in pH 6.7 and 7.8 solutions were both capable of bearing loads, and no significant mechanical differences were observed between the two pH conditions (Figures 4, S7). This is consistent with the formation of bis- and tris-coordinated metal ion coordination and presence of bidentate bonding and covalent crosslinking due to pH-dependent oxidation reactions.<sup>33</sup> Such pH-dependent crosslinking has previously been reported within the cuticle, which is composed primarily of mfp-1<sup>39,41</sup>. Our results suggest that pore formation and/or pH-dependent crosslinking of the cuticle or plaque interior contributes to the formation of rigid structures<sup>14</sup>, as well as the development of mechanical strength and adhesion. Interestingly, there is empirical evidence that this mechanical property development takes some time. We have noted that for mature plaques, formaldehyde-based crosslinking prior to cryo-sectioning is not necessary and the plaque structures are identical with and without fixation. However, freshly-deposited plaques are considerably softer and sectioning and observation without fixation is difficult.

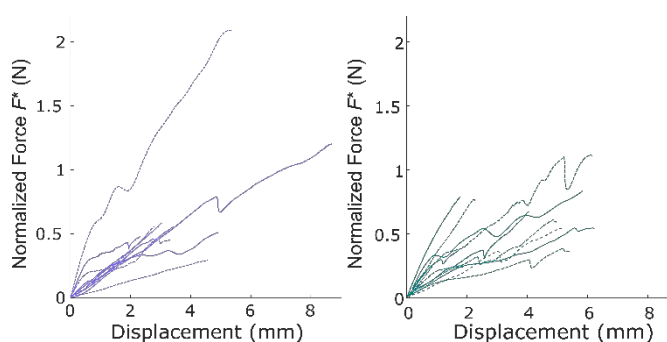


**Figure 4.** Tensile data showing (left) pH 6.7 vs. (right) pH 7.8. Forces at pH 3.0 were too low to detect. Solid lines indicate failures at the thread; dotted lines indicate adhesive failures.

Previous work on pH-dependencies for mussel tenacity focused on deposition conditions only, and provided mixed results. One study noted considerable differences in the mechanical properties of byssal threads by changing pH by as little as 0.2 from pH  $\sim 8.2$  to pH  $\sim 8.0$  by varying the atmospheric  $p_{\text{CO}_2}$  levels within the mussel tanks during deposition<sup>42</sup>. Real time PCR results suggested this effect could be attributed to changes in gene expression prior to mfp secretion<sup>43</sup>. A more recent study failed to observe mechanical property differences between threads deposited at pH 7.98 and 7.47<sup>44</sup>. Our experiments are distinct in that we examine the plaque specifically, with respect to the effects of extended exposure to solutions of varying pH.

## 4 Conclusions

Taken together, our results support a model in which a coacervate phase, rich in mfps, is generated under the mussel foot, then undergoes a pH dependent phase change accompanied by crosslinking to establish both multiscale structural features and mechanical strength. At low pH, porous microstructures fail to form, and the plaques are feeble. The lack of pores may indicate a failure to form the metastable coacervate phase, or a failure to sustain phase inversion. It is likely that at low pH only weak electrostatic interactions are present, decreasing the adhesive and cohesive capabilities of the plaque. At pH values of 6.7 or 7.8, we observe robust formation of porous microstructures and measure significant tensile strengths. These findings demonstrate the importance of pH change on the development of marine mussel plaques and provide insight into the stepwise order of bioprocessing that occurs during deposition.

## Conflicts of interest

There are no conflicts to declare.

## Acknowledgements

This work was supported by the MRSEC Program of the National Science Foundation under Award No. DMR 1720256 (IRG-3). The authors acknowledge the use of the Mechanical Test Laboratory of the UCSB Mechanical Engineering Department, the UCSB NRI-MCDB Microscopy Facility, the Microfluidics Laboratory within the California NanoSystems Institute, supported by the University of California, Santa Barbara and the University of California, Office of the President, and the MRL Shared Experimental Facilities that are supported by the MRSEC Program of the NSF under Award No. DMR 1720256; a member of the NSF-funded Materials Research Facilities Network. We thank G. Chandler Bartz and Daniel G. DeMartini for assistance in the initial set-up of the experiment. JHB acknowledges support of the Summer Undergraduate Research Fellowship and the Research Internships in Science and Engineering programs through the UCSB College of Creative Studies, and MRSEC, respectively. EF acknowledges funding support from the Otis Williams Postdoctoral Fellowship.

## References

- N. Cohen, J. H. Waite, R. M. McMeeking and M. T. Valentine, *Philos. Trans. R. Soc., B*, 2019, **374**, 20190202.
- E. Filippidi, D. G. DeMartini, P. M. d. Molina, E. W. Danner, J. Kim, M. E. Helgeson, J. H. Waite and M. T. Valentine, *J. R. Soc., Interface*, 2015, **12**, 20150827.
- B. P. Lee, P. B. Messersmith, J. N. Israelachvili and J. H. Waite, *Annu. Rev. Mater. Res.*, 2011, **41**, 99-132.
- C. A. Monnier, D. G. DeMartini and J. H. Waite, *Nat. Commun.*, 2018, **9**, 3424.
- D. J. Crisp, G. Walker, G. A. Young and A. B. Yule, *J. Colloid Interface Sci.*, 1985, **104**, 40-50.
- J. H. Waite, *Biol. Rev.*, 1983, **58**, 209-231.
- E. Bell and J. Gosline, *J. Exp. Biol.*, 1996, **199**, 1005.
- L. Petrone, A. Kumar, C. N. Sutanto, N. J. Patil, S. Kannan, A. Palaniappan, S. Amini, B. Zappone, C. Verma and A. Miserez, *Nat. Commun.*, 2015, **6**, 8737.
- K. W. Desmond, N. A. Zacchia, J. H. Waite and M. T. Valentine, *Soft Matter*, 2015, **11**, 6832-6839.
- M. H. Wilhelm, E. Filippidi, J. H. Waite and M. T. Valentine, *Soft Matter*, 2017, **13**, 7381-7388.
- A. Tamarin and P. Keller, *J. Ultrastruct. Res.*, 1972, **40**, 401-416.
- A. Tamarin, P. Lewis and J. Askey, *J. Morphol.*, 1976, **149**, 199-221.
- J. H. Waite, in *Structure, cellular synthesis and assembly of biopolymers*, Springer, 1992, pp. 27-54.
- L. V. Zuccarello, *J. Ultrastruct. Res.*, 1980, **73**, 135-147.
- J. H. Waite, *J. Exp. Biol.*, 2017, **220**, 517-530.
- T. Priemel, E. Degtyar, M. N. Dean and M. J. Harrington, *Nat. Commun.*, 2017, **8**, 14539.
- N. R. Martinez Rodriguez, S. Das, Y. Kaufman, J. N. Israelachvili and J. H. Waite, *Biofouling*, 2015, **31**, 221-227.
- J. Yu, W. Wei, E. Danner, R. K. Ashley, J. N. Israelachvili and J. H. Waite, *Nat. Chem. Biol.*, 2011, **7**, 588-590.
- D. R. Miller, J. E. Spahn and J. H. Waite, *J. R. Soc., Interface*, 2015, **12**, 20150614.
- D. G. DeMartini, J. M. Errico, S. Sjoestroem, A. Fenster and J. H. Waite, *J. R. Soc., Interface*, 2017, **14**, 20170151.
- W. Wei, Y. Tan, N. R. Martinez Rodriguez, J. Yu, J. N. Israelachvili and J. H. Waite, *Acta Biomater.*, 2014, **10**, 1663-1670.
- H. B. De Jong, in *Colloid science*, Elsevier Amsterdam, 1949, vol. 2, pp. 335-432.
- D. S. Hwang, H. Zeng, A. Srivastava, D. V. Krogstad, M. Tirrell, J. N. Israelachvili and J. H. Waite, *Soft Matter*, 2010, **6**, 3232-3236.
- I. Kaminker, W. Wei, A. M. Schrader, Y. Talmon, M. T. Valentine, J. N. Israelachvili, J. H. Waite and S. Han, *Soft Matter*, 2017, **13**, 9122-9131.
- D. R. Miller, S. Das, K.-Y. Huang, S. Han, J. N. Israelachvili and J. H. Waite, *ACS Biomater. Sci. Eng.*, 2015, **1**, 1121-1128.
- S. Lim, Y. S. Choi, D. G. Kang, Y. H. Song and H. J. Cha, *Biomaterials*, 2010, **31**, 3715-3722.
- J. Wang and T. Scheibel, *Biomacromolecules*, 2018, **19**, 3612-3619.
- E. Valois, R. Mirshafian and J. H. Waite, *Sci. Adv.*, 2020, **6**, eaaz6486.
- H. Strathmann and K. Kock, *Desalination*, 1977, **21**, 241-255.
- S. Mazinani, S. Darvishmanesh, A. Ehsanzadeh and B. Van der Bruggen, *J. Membr. Sci.*, 2017, **526**, 301-314.
- D. R. Tree, K. T. Delaney, H. D. Ceniceros, T. Iwama and G. H. Fredrickson, *Soft Matter*, 2017, **13**, 3013-3030.
- H. G. Silverman and F. F. Roberto, *Mar. Biotechnol.*, 2007, **9**, 661-681.
- N. Holten-Andersen, M. J. Harrington, H. Birkedal, B. P. Lee, P. B. Messersmith, K. Y. C. Lee and J. H. Waite, *Proc. Natl. Acad. Sci. U. S. A.*, 2011, **108**, 2651-2655.
- J. Yu, Y. Kan, M. Rapp, E. Danner, W. Wei, S. Das, D. R. Miller, Y. Chen, J. H. Waite and J. N. Israelachvili, *Proc. Natl. Acad. Sci. U. S. A.*, 2013, **110**, 15680-15685.
- J. Yu, W. Wei, M. S. Menyo, A. Masic, J. H. Waite and J. N. Israelachvili, *Biomacromolecules*, 2013, **14**, 1072-1077.

36. L. M. Rzepecki, K. M. Hansen and J. H. Waite, *Biol. Bull.*, 1992, **183**, 123-137.
37. Q. Zhao, D. W. Lee, B. K. Ahn, S. Seo, Y. Kaufman, J. N. Israelachvili and J. H. Waite, *Nat. Mater.*, 2016, **15**, 407-412.
38. C. M. Duarte, I. E. Hendriks, T. S. Moore, Y. S. Olsen, A. Steckbauer, L. Ramajo, J. Carstensen, J. A. Trotter and M. McCulloch, *Estuaries Coasts*, 2013, **36**, 221-236.
39. N. Holten-Andersen, T. E. Mates, M. S. Toprak, G. D. Stucky, F. W. Zok and J. H. Waite, *Langmuir*, 2009, **25**, 3323-3326.
40. S. W. Taylor, J. H. Waite, M. M. Ross, J. Shabanowitz and D. F. Hunt, *J. Am. Chem. Soc.*, 1994, **116**, 10803-10804.
41. C. Sun and J. H. Waite, *J. Biol. Chem.*, 2005, **280**, 39332-39336.
42. M. J. O'Donnell, M. N. George and E. Carrington, *Nat. Clim. Change*, 2013, **3**, 587-590.
43. X. Zhao, C. Guo, Y. Han, Z. Che, Y. Wang, X. Wang, X. Chai, H. Wu and G. Liu, *Mar. Ecol.: Prog. Ser.*, 2017, **565**, 67-77.
44. G. Dickey, B. M. Preziosi, C. T. Clark and T. J. Bowden, *PLoS One*, 2018, **13**, e0205908-e0205908.